A Three Step Reaction Model of Smoldering and Flaming Combustion

Emma Hart

December 2021

Abstract

Smoldering and flaming are two intimately related combustion processes, but they lend themselves well to being modeled separately rather than together, especially because of the different mediums in which the two take place. A single model that could describe both types of combustion may be helpful in giving insight into the relationship and transition between the two. To this end, in this paper, I consider smoldering and flaming combustion together with a three step opposed flow reaction model. I create and nondimensionalize a system of partial differential equations, and consider traveling wave solutions by converting it to a moving coordinate system. The model is simulated numerically using finite difference schemes. It was found that this model is able to support both smoldering and flaming solutions, though the context may be quite limited by time-step size. I also evaluate the effects of the assumption that gas heat capacities are equal, and find that important characteristics of the system may be lost with this assumption.

1 Introduction

Smoldering combustion, characterized by the slow, low temperature, flameless burning of solid fuel, is the most persistent type of combustion. In contrast, flaming combustion, involving a higher temperature burning of gaseous fuel, is rather limited in how long it can be sustained. Smoldering combustion reactions can last on the scale of months, years, or even decades [7]. Smoldering combustion is an important topic of study in engineering, ecology, and earth science contexts, among others, as it poses significant threats in many varied contexts, including residential fires, the destruction of biomass in soil, and the release of air pollution from long-stored carbon sources in the earth [6].

Because smoldering combustion involves thousands of unknown and context-specific chemical reactions, most models consider the process as happening in one or more general reaction steps. Depending on the topic or behavior of interest, these steps may be combined or distinguished in different ways. Model steps most often include the oxidation of some fuel(s) – that could include virgin solid fuel, char, and/or flammable gases – and may also include pyrolysis. Pyrolysis is an endothermic process in which solid fuel is heated and thereby transformed into more combustible products of char and flammable gases. More heat is produced from the oxidation of char than the oxidation of virgin solid fuel, and even more heat is produced from the oxidation of flammable gases. With these kinds of reaction steps, carefully chosen models can still describe complex qualitative behaviors of interest with simple terms, and further, they can help give intuition into combustive processes.

Smoldering models are also often specifically designed to consider just one direction of incoming gas relative to the direction of the propagating smoldering wave. This is important because smoldering combustion involves reactions that take place in both solid and gaseous phases. A process in which the direction of incoming gases is one way can be spatially quite different from the process when incoming gases are moving the opposite way. Co-flow smolder models (also called forward or counter-current smolder models), describe systems in which the propagating front and incoming gases travel in the same direction. In this case, fresh solid fuel and oxygen effectively meet from opposite directions and must mix for fuel oxidation to occur. The more studied type of smolder is opposed-flow smolder (also called reverse, counter-flow, or co-current smolder), in which the direction of incoming gases is opposite to the direction of the smolder wave. In this case, fresh solid fuel and oxygen are premixed such that a model considering a single reaction site, in which all reactants are mixed, may reasonably capture the system's behavior.

Opposed-flow and co-flow smoldering models have been well explored numerically. Decker and Schult [3], for example, consider the extinction of an opposed-flow smoldering wave in a single step reaction in relation to high air flow above a critical value (over-blowing). Although they note that simplifications in considering only a single step are likely to affect quantitative results, their model efficiently describes qualitative results: pulsations that occur in over-blowing conditions. Kelley and Schult [4] complicate the reaction model by adding a second reaction step to address a discrepancy between the extinction behaviors predicted by numerical models and those seen experimentally. Lu [5], similar to Decker and Schult [3], develops a one step reaction model but investigates co-flow smolder, rather than opposed-flow, to examine heat loss effects.

Although smoldering and flaming combustion are intimately related, often occurring at the same time in

wild fires and feeding into one another in especially dangerous ways, literature describing smoldering combustion is somewhat sparsely connected to the literature describing flaming combustion [7]. Understanding the relationships between smoldering and flaming and the transition between the two is especially important in fire safety, as understanding the fundamental mechanisms of transition could help to understand how to better control smoldering and flaming.

Aldushin et al. [1] numerically investigate this transition with a three-step reaction process for opposed-flow smolder, including fuel oxidation, pyrolysis, and char oxidation in a planar model. They define the flaming distance – the distance that a smolder wave progresses before the char oxidation reaction spontaneously self accelerates – as a measure of particular importance in transition. Further, they find that although char oxidation hardly affects how the smoldering wave propagates, under appropriate conditions, it can act as the trigger for the transition to flaming. This model does not include a reaction step for the burning of gaseous fuel that characterizes flaming combustion; rather, they treat a rapid and significant increase in temperature as a transition to flaming.

Experimental results further give insight into what the key steps in the transition from smoldering to flaming may be. Bar-Ilan et al. [2], in microgravity experiments on small samples, find that decreasing the flow velocity and increasing oxygen concentration makes samples more likely to transition to flaming. From analyzing results of experimentation on foam and fabric samples, Stoliarov et al. [9] speculate that the formation of adjacent pyrolysis and smoldering regions is especially important to consider in the transition to flaming [9]. The heat and chemical products from these regions can combine to sustain the pyrolysis and smoldering reactions and/or to transition to flaming. The pyrolysis region produces a gaseous fuel from an endothermic reaction. The smoldering region can produce the heat necessary to sustain pyrolysis and to ignite the gaseous fuel products of the pyrolysis region, leading to flaming.

2 Mathematical Model

Building on these results, in this project, I aim to develop a model that can describe both smoldering and flaming combustion to give insight into this transition. Because smoldering combustion involves a solid/gas reaction, whereas flaming combustion involves only a gaseous reaction, this model must include at least two steps. I will consider a three step reaction process for opposed-flow smolder, including pyrolysis/fuel

oxidation, char oxidation, and gas oxidation:

$$\text{oxygen} + \text{solid fuel} \rightarrow \text{char} + \text{flammable gas} \tag{1}$$

$$\text{oxygen} + \text{char} \rightarrow \text{ash} + \text{smoke} \tag{2}$$

$$\text{oxygen} + \text{flammable gas} \rightarrow \text{smoke}. \tag{3}$$

The first step (1) involves both pyrolysis and fuel oxidation with the combination of oxygen and solid fuel producing char and flammable gases. Some models, including the model formulated in [1], separate the two fuel oxidation and pyrolysis reactions. The two differ in that pyrolysis is characterized by an endothermic heating of a solid fuel sample to produce char and flammable gases, while fuel oxidation is the exothermic process of an oxidizer combining with solid fuel to produce char. In certain contexts, it can be helpful to distinguish the two, however in analyzing the transition to flaming, it is anticipated in this context that the two processes are so linked that there would be little relevance in distinguishing them. This could be a site of future/possible work, and, if a reason were found in numerical experiments to separate them, this addition should be straightforward to implement.

Char oxidation (2) involves the combination of oxygen with the char produced from pyrolysis, producing ash and smoke. This is an exothermic process, and both the ash and smoke products are treated as nonreactive in following reaction steps. Gas oxidation (3) involves the combination of oxygen and the flammable gaseous products of pyrolysis, producing smoke. This is a highly exothermic process, producing much more heat than reaction (2) (on the scale of ten times as much). Smoldering is defined by reactions (1) and (2), where combustion remains within the porous solid medium, while flaming is defined by reactions (1) and (3), where combustion occurs between gaseous components.

From the consideration of these three steps as those most integral in the transition between smoldering and flaming come the following equations. These equations describe the conservation of energy; the conservation of fuel, char, ash, gas, oxidizer, and flammable gas masses; the conservation of gas momentum via Darcy's law for the movement of gas through a porous medium; and the ideal gas law as the equation of state. These are described in terms of variables for temperature T; pressure P; gas velocity v_g; the reaction rates of the first, second, and third reactions W_1, W_2, and W_1; density of solid fuel ρ_f, char ρ_c, ash ρ_a, and total gas ρ_g; the oxygen gas fraction Y; the flammable gas fraction F; the smoke fraction S; space x; and time t. Note

that tildes represent dimensional versions of these terms.

Reaction Rates:

$$\tilde{W_1} = \tilde{K_1}\tilde{P}Y\tilde{\rho_f}e^{-\frac{\tilde{E_1}}{\tilde{R}\tilde{T}}} \tag{4}$$

$$\tilde{W_2} = \tilde{K_2}\tilde{P}Y\tilde{\rho_c}e^{-\frac{\tilde{E_2}}{\tilde{R}\tilde{T}}} \tag{5}$$

$$\tilde{W_3} = \tilde{K_3}\tilde{P}^2YFe^{-\frac{\tilde{E_3}}{\tilde{R}\tilde{T}}} \tag{6}$$

Energy:

$$\frac{\partial\tilde{C}\tilde{T}}{\partial\tilde{t}} + \frac{\partial\tilde{M}\tilde{T}}{\partial\tilde{x}} = \tilde{\lambda}\frac{\partial^2\tilde{T}}{\partial\tilde{x}^2} + \tilde{Q_1}\tilde{W_1} + \tilde{Q_2}\tilde{W_2} + \tilde{Q_3}\tilde{W_3} \tag{7}$$

Fuel Mass:

$$\frac{\partial\tilde{\rho_f}}{\partial\tilde{t}} = -\tilde{W_1} \tag{8}$$

Char Mass:

$$\frac{\partial\tilde{\rho_c}}{\partial\tilde{t}} = \mu_{c1}\tilde{W_1} - \tilde{W_2} \tag{9}$$

Ash Mass:

$$\frac{\partial\tilde{\rho_a}}{\partial\tilde{t}} = \mu_{a2}\tilde{W_2} \tag{10}$$

Total Gas Mass:

$$\frac{\partial\tilde{\rho_g}}{\partial\tilde{t}} + \frac{\partial\tilde{\rho_g}\tilde{v_g}}{\partial\tilde{x}} = (\mu_{c1}-1)\tilde{W_1} + (\mu_{a2}-1)\tilde{W_2} + (\mu_{sm3}-1)\tilde{W_3} \tag{11}$$

Oxidizer Mass:

$$\frac{\partial\tilde{\rho_g}Y}{\partial\tilde{t}} + \frac{\partial\tilde{\rho_g}\tilde{v_g}Y}{\partial\tilde{x}} = \tilde{D_{ox}}\tilde{\rho_g}\frac{\partial^2Y}{\partial\tilde{x}^2} - \mu_{ox1}\tilde{W_1} - \mu_{ox2}\tilde{W_2} - \mu_{ox3}\tilde{W_3} \tag{12}$$

Flammable Gas Mass:

$$\frac{\partial\tilde{\rho_g}F}{\partial\tilde{t}} + \frac{\partial\tilde{\rho_g}\tilde{v_g}F}{\partial\tilde{x}} = \tilde{D_{fg}}\tilde{\rho_g}\frac{\partial^2F}{\partial\tilde{x}^2} + \mu_{fg1}\tilde{W_1} - \tilde{W_3} \tag{13}$$

Smoke Mass:

$$\frac{\partial\tilde{\rho_g}S}{\partial\tilde{t}} + \frac{\partial\tilde{\rho_g}\tilde{v_g}S}{\partial\tilde{x}} = \tilde{D_{sm}}\tilde{\rho_g}\frac{\partial^2F}{\partial\tilde{x}^2} + \mu_{sm2}\tilde{W_2} + \mu_{sm3}\tilde{W_3} \tag{14}$$

Gas Momentum:

$$\frac{\partial\tilde{P}}{\partial\tilde{x}} = -\tilde{k_f}\tilde{v_g} \tag{15}$$

Equation of State:

$$\tilde{P} = \tilde{\rho_g}\tilde{R}\tilde{T} \tag{16}$$

While in similar models the specific heat capacities of all gases are often considered equal, we introduce a weighted heat capacity term

$$\tilde{C} = \tilde{c_f}\tilde{\rho_f} + \tilde{c_c}\tilde{\rho_c} + \tilde{c_a}\tilde{\rho_a} + \tilde{c_{ox}}Y\tilde{\rho_g} + \tilde{c_{fg}}F\tilde{\rho_g} + \tilde{c_{sm}}S\tilde{\rho_g} + \tilde{c_i}(1-Y-F-S)\tilde{\rho_g} \tag{17}$$

that represents the specific heat capacity of all gases mixed in the system. Additionally, we introduce the weighted heat capacity of all material flux:

$$\tilde{M} = \tilde{\rho_g}\tilde{v_g}[\tilde{c_{ox}}Y + \tilde{c_{fg}}F + \tilde{c_{sm}}S + \tilde{c_i}(1-Y-F-S)]. \tag{18}$$

Both change depending on the concentrations of oxygen, flammable gases produced by pyrolysis, smoke, and inert gases in the system, thereby allowing us to consider how the differing specific heat capacities of these gases may affect the dynamics of this system. However, we still consider these specific heat capacities to be constant with temperature.

From the assumption that heat capacity is conserved, we further find:

$$\tilde{c_f} + \mu_{ox1}\tilde{c_{ox}} = \mu_{c1}\tilde{c_c} + \mu_{fg1}\tilde{c_{fg}}, \qquad \tilde{c_c} + \mu_{ox2}\tilde{c_{ox}} = \mu_{a2}\tilde{c_a} + \mu_{sm2}\tilde{c_{sm}}, \qquad \tilde{c_{fg}} + \mu_{ox3}\tilde{c_{ox}} = \mu_{sm3}\tilde{c_{sm}}. \tag{19}$$

Stoichiometric parameters include: the ratios of the char mass μ_{c1} , flammable gas mass μ_{fg1}, oxidizer mass μ_{ox1}, and net gas mass $\mu_{c1} - 1$ produced or consumed per unit mass of solid fuel (via reaction 1); the ratios of ash mass μ_{a2}, oxidizer mass μ_{ox2}, smoke mass μ_{sm2}, and net gas mass $\mu_{a2} - 1$ produced or consumed per unit mass of char (via reaction 2); and the ratios of oxidizer mass μ_{ox3}, smoke mass μ_{sm3}, and total gas mass $\mu_{sm3} - 1$ produced or consumed per unit flammable gas (via reaction 3). Other parameters include: the pre-exponential terms for each of the three steps K_1, K_2, and K_3; their activation energies E_1, E_2, and E_3; their heats of reaction Q_1, Q_2, and Q_3; the heat capacities of the solid fuel c_f, char c_c, ash c_a, oxygen c_{ox}, flammable gases c_{fg}, smoke c_{sm}, and inert gases c_i; a friction coefficient for the flow through a porous medium k_f; the thermal conductivity coefficient λ; and diffusion coefficients for oxygen, flammable gases, and smoke D_{ox}, D_{fg}, and D_{sm}. While these D terms and ρ_g vary with temperature, we treat their product as constant in space, time, and with varying temperature, following [4]. The thermal conductivity coefficient λ is also considered constant in space. Additional simplifications include assumptions of the Arrhenius reaction rate dependence on temperature, the ideal gas law, Darcy's law for fluid flow through a porous medium, and an adiabatic system with no heat losses. Though these simplifications are likely to have numerical effects,

the described processes of transition are still likely to occur.

Boundary conditions for opposed-flow smolder of a sample of length ℓ are given by:

$$\tilde{x}=0: \quad \tilde{P}=\tilde{P}_0 \quad \tilde{T}=\tilde{T}_0 \quad Y=Y_0 \quad F=0 \quad S=0 \quad \tilde{\rho_g}\tilde{v_g}=\tilde{J} \quad \tilde{\rho_f}=1 \quad \tilde{\rho_c}=0 \quad \tilde{\rho_a}=0 \tag{20}$$

$$\tilde{x}=\tilde{\ell}: \quad \frac{\partial T}{\partial \tilde{x}}=0 \quad \frac{\partial Y}{\partial \tilde{x}}=0 \quad \frac{\partial F}{\partial \tilde{x}}=0 \quad \frac{\partial S}{\partial \tilde{x}}=0 \tag{21}$$

where T_0 is the ambient temperature, P_0 is the ambient pressure, Y_0 is the fraction of oxygen in surrounding air, and J is the gas mass flux.

2.1 Nondimensionalization

To reduce parameters, I nondimensionalize the set of equations with the following nondimensional variables,

$$\hat{x}=\frac{\tilde{x}}{\tilde{x_*}}, \qquad \hat{t}=\frac{\tilde{t}}{\tilde{t_*}}, \qquad P=\frac{\tilde{P}}{\tilde{P_0}}, \qquad v_g=\frac{\tilde{v_g}\tilde{t_*}}{\tilde{x_*}}, \qquad C=\frac{\tilde{C}}{\tilde{c_i}},$$

$$\rho_g=\frac{\tilde{\rho_g}}{\tilde{\rho_g^0}}, \qquad \rho_f=\frac{\tilde{\rho_f}}{\tilde{\rho_f^0}}, \qquad \rho_c=\frac{\tilde{\rho_c}}{\tilde{\rho_f^0}}, \qquad \rho_a=\frac{\tilde{\rho_a}}{\tilde{\rho_f^0}},$$

$$W_1=\frac{\tilde{t_*}}{\tilde{\rho_f^0}}\tilde{W}_1, \qquad W_2=\frac{\tilde{t_*}}{\tilde{\rho_f^0}}\tilde{W}_2, \qquad W_3=\frac{\tilde{t_*}}{\tilde{\rho_g^0}}\tilde{W}_3, \qquad \theta=\frac{\tilde{T}-\tilde{T}_0}{\tilde{T}_*-\tilde{T}_0},$$

$$\theta_C=C\left(\frac{1+\delta\theta}{\delta}\right), \qquad C=\frac{\tilde{C}}{\tilde{\rho_f^0}\tilde{c_f}}, \qquad M=\frac{\tilde{M}\tilde{t_*}}{\tilde{\rho_g^0}\tilde{c_i}\tilde{x_*}},$$

and the following parameters,

$$\tilde{x_*}^2=\frac{\tilde{\lambda}\tilde{t_*}}{\tilde{\rho_f^0}\tilde{c_f}}, \qquad \tilde{t_*}=\frac{1}{\tilde{K_1}\tilde{P_0}}e^{\frac{\tilde{E_1}}{\tilde{R}\tilde{T_*}}}, \qquad \tilde{P_0}=\tilde{\rho_g^0}\tilde{R}\tilde{T_0},$$

$$\tilde{T_*}=\tilde{T_0}+\frac{\tilde{\rho_f^0}\tilde{Q_1}+\tilde{\rho_g^0}\mu_{fg1}\tilde{Q_3}}{\tilde{\rho_f^0}\tilde{c_f}}, \qquad \bar{\rho}=\frac{\tilde{\rho_f^0}}{\tilde{\rho_g^0}}, \qquad \bar{c}=\frac{\tilde{c_f}}{\tilde{c_i}},$$

$$Z_1=\frac{\tilde{E_1}(\tilde{T_*}-\tilde{T_0})}{\tilde{R}\tilde{T_*}^2}, \qquad Z_2=\frac{\tilde{E_2}(\tilde{T_*}-\tilde{T_0})}{\tilde{R}\tilde{T_*}^2}, \qquad Z_3=\frac{\tilde{E_3}(\tilde{T_*}-\tilde{T_0})}{\tilde{R}\tilde{T_*}^2},$$

$$Kr_{2,1}=\frac{\tilde{K_2}e^{\frac{-\tilde{E_2}}{\tilde{R}\tilde{T_*}}}}{\tilde{K_1}e^{\frac{-\tilde{E_1}}{\tilde{R}\tilde{T_*}}}}, \qquad Kr_{3,1}=\frac{\tilde{K_3}\tilde{P_0}e^{\frac{-\tilde{E_3}}{\tilde{R}\tilde{T_*}}}}{\tilde{K_1}\tilde{\rho_g^0}e^{\frac{-\tilde{E_1}}{\tilde{R}\tilde{T_*}}}}, \qquad \delta=\frac{\tilde{T_*}-\tilde{T_0}}{\tilde{T_0}}, \qquad k_f=\frac{\tilde{k_f}\tilde{x_*}^2}{\tilde{P_0}\tilde{t_*}}$$

$$Q_1=\frac{\tilde{Q_1}}{\tilde{c_f}(\tilde{T_*}-\tilde{T_0})}, \qquad Q_2=\frac{\tilde{Q_2}}{\tilde{c_f}(\tilde{T_*}-\tilde{T_0})}, \qquad Q_3=\frac{\tilde{Q_3}}{\tilde{c_i}(\tilde{T_*}-\tilde{T_0})},$$

$$Le_{ox}=\frac{\tilde{x_*}^2}{\tilde{D_{ox}}\tilde{t_*}\tilde{\rho_g}}, \qquad Le_{fg}=\frac{\tilde{x_*}^2}{\tilde{D_{fg}}\tilde{t_*}\tilde{\rho_g}}, \qquad Le_{sm}=\frac{\tilde{x_*}^2}{\tilde{D_{sm}}\tilde{t_*}\tilde{\rho_g}},$$

$$c_c=\frac{\tilde{c_c}}{\tilde{c_f}}, \qquad c_a=\frac{\tilde{c_a}}{\tilde{c_f}}, \qquad c_{ox}=\frac{\tilde{c_{ox}}}{\tilde{c_i}}, \qquad c_{fg}=\frac{\tilde{c_{fg}}}{\tilde{c_i}}, \qquad c_{sm}=\frac{\tilde{c_{sm}}}{\tilde{c_i}}.$$

Note that while the pre-exponential terms $\tilde{K_1}$ and $\tilde{K_2}$ share the same dimensions, because Reaction (3) involves no solid reactants, $\tilde{K_3}$ does not; the dimensional product $\tilde{P}_0/\tilde{\rho}_g^0$ thus appears in the nondimensional constant $Kr_{3,1}$ because the ratio $\tilde{K_1}/\tilde{K_3}$ is also dimensional (with the same dimensions as $\tilde{P}_0/\tilde{\rho}_g^0$).

This all results in the following nondimensional equations:

$$W_1 = PY\rho_f e^{Z_1(\theta-1)\frac{1+\delta}{1+\delta\theta}} \tag{22}$$

$$W_2 = Kr_{2,1}PY\rho_c e^{Z_2(\theta-1)\frac{1+\delta}{1+\delta\theta}} \tag{23}$$

$$W_3 = Kr_{3,1}P^2YFe^{Z_3(\theta-1)\frac{1+\delta}{1+\delta\theta}} \tag{24}$$

$$\frac{\partial\theta_C}{\partial\hat{t}} + \frac{1}{\bar{\rho}\bar{c}}\frac{\partial\left(\frac{M}{C}\right)\theta_C}{\partial\hat{x}} = \frac{\partial^2\left(\frac{1}{C}\right)\theta_C}{\partial\hat{x}^2} + Q_1W_1 + Q_2W_2 + \frac{1}{\bar{\rho}\bar{c}}Q_3W_3 \tag{25}$$

$$\frac{\partial\rho_f}{\partial\hat{t}} = -W_1 \tag{26}$$

$$\frac{\partial\rho_c}{\partial\hat{t}} = \mu_{c1}W_1 - W_2 \tag{27}$$

$$\frac{\partial\rho_a}{\partial\hat{t}} = \mu_{a2}W_2 \tag{28}$$

$$\frac{\partial\rho_g}{\partial\hat{t}} + \frac{\partial\rho_g v_g}{\partial\hat{x}} = \bar{\rho}(\mu_{c1}-1)W_1 + \bar{\rho}(\mu_{a2}-1)W_2 + (\mu_{sm3}-1)W_3 \tag{29}$$

$$\frac{\partial\rho_g Y}{\partial\hat{t}} + \frac{\partial\rho_g v_g Y}{\partial\hat{x}} = \frac{1}{Le_{ox}}\frac{\partial^2 Y}{\partial\hat{x}^2} - \mu_{ox1}\bar{\rho}W_1 - \mu_{ox2}\bar{\rho}W_2 - \mu_{ox3}W_3 \tag{30}$$

$$\frac{\partial\rho_g F}{\partial\hat{t}} + \frac{\partial\rho_g v_g}{F}\partial\hat{x} = \frac{1}{Le_{fg}}\frac{\partial^2 F}{\partial\hat{x}^2} + \mu_{fg1}\bar{\rho}W_1 - W_3 \tag{31}$$

$$\frac{\partial\rho_g S}{\partial\hat{t}} + \frac{\partial\rho_g v_g S}{\partial\hat{x}} = \frac{1}{Le_{sm}}\frac{\partial^2 S}{\partial\hat{x}^2} + \mu_{sm2}\bar{\rho}W_2 + \mu_{sm3}W_3 \tag{32}$$

$$\frac{\partial P}{\partial\hat{x}} = -k_f v_g \tag{33}$$

$$P = \rho_g(1+\delta\theta) \tag{34}$$

The expressions in Equation 19 can be nondimensionalized and rewritten as:

$$\mu_{ox1} = \frac{\mu_{c1}c_c + \bar{c}\mu_{fg1}c_{fg} - 1}{\bar{c}c_{ox}}, \qquad \mu_{ox2} = \frac{\mu_{a2}c_a + \bar{c}\mu_{sm2}c_{sm} - c_c}{\bar{c}c_{ox}}, \qquad \mu_{ox3} = \frac{\mu_{sm3}c_{sm} - c_{fg}}{c_{ox}} \tag{35}$$

The boundary conditions for the nondimensionalized equations are given by:

$$\hat{x}=0: \quad P=1 \quad \theta=0 \quad Y=Y_0 \quad F=0 \quad S=0 \quad \rho_g v_g = J \quad \rho_f = 1 \quad \rho_c = 0 \quad \rho_a = 0 \tag{36}$$

$$\hat{x}=\frac{\ell}{\tilde{x_*}}=\ell: \quad \frac{\partial \theta}{\partial \hat{x}}=0 \quad \frac{\partial Y}{\partial \hat{x}}=0 \quad \frac{\partial F}{\partial \hat{x}}=0 \quad \frac{\partial S}{\partial \hat{x}}=0 \tag{37}$$

2.2 Moving Coordinate System

A uniformly propagating wave would appear as a solution independent of time in a moving coordinate system that travels with the same constant speed as the wave. I therefore introduce a moving coordinate system of the form $x = \hat{x} + u\hat{t}$, $t = \hat{t}$, as in [3], [4], and [8], to consider these traveling wave solutions. Here, I define $\rho_f = \frac{1}{2}$ at $x = 0$, representing the position of the reaction zone. The coefficient u represents the speed of the propagating wave. This is constant in space, but may vary in time with pulsations of the wave. The equations converted to the moving coordinate system become:

$$W_1 = PY\rho_f e^{Z_1(\theta-1)\frac{1+\delta}{1+\delta\theta}} \tag{38}$$

$$W_2 = Kr_{2,1}PY\rho_c e^{Z_2(\theta-1)\frac{1+\delta}{1+\delta\theta}} \tag{39}$$

$$W_3 = Kr_{3,1}P^2YFe^{Z_3(\theta-1)\frac{1+\delta}{1+\delta\theta}} \tag{40}$$

$$\frac{\partial \theta_C}{\partial t} + u\frac{\partial \theta_C}{\partial x} + \frac{1}{\bar{\rho}\bar{c}}\frac{\partial\left(\frac{M}{C}\right)\theta_C}{\partial x} = \frac{\partial^2\left(\frac{1}{C}\right)\theta_C}{\partial x^2} + Q_1W_1 + Q_2W_2 + \frac{1}{\bar{\rho}\bar{c}}Q_3W_3 \tag{41}$$

$$\frac{\partial \rho_f}{\partial t} + u\frac{\partial \rho_f}{\partial x} = -W_1 \tag{42}$$

$$\frac{\partial \rho_c}{\partial t} + u\frac{\partial \rho_c}{\partial x} = \mu_{c1}W_1 - W_2 \tag{43}$$

$$\frac{\partial \rho_a}{\partial t} + u\frac{\partial \rho_a}{\partial x} = \mu_{a2}W_2 \tag{44}$$

$$\frac{\partial \rho_g}{\partial t} + u\frac{\partial \rho_g}{\partial x} + \frac{\partial \rho_g v_g}{\partial x} = \bar{\rho}(\mu_{c1}-1)W_1 + \bar{\rho}(\mu_{a2}-1)W_2 + (\mu_{sm3}-1)W_3 \tag{45}$$

$$\frac{\partial \rho_g Y}{\partial t} + u\frac{\partial \rho_g Y}{\partial x} + \frac{\partial \rho_g v_g Y}{\partial x} = \frac{1}{Le_{ox}}\frac{\partial^2 Y}{\partial x^2} - \mu_{ox1}\bar{\rho}W_1 - \mu_{ox2}\bar{\rho}W_2 - \mu_{ox3}W_3 \tag{46}$$

$$\frac{\partial \rho_g F}{\partial t} + u\frac{\partial \rho_g F}{\partial x} + \frac{\partial \rho_g v_g F}{\partial x} = \frac{1}{Le_{fg}}\frac{\partial^2 F}{\partial x^2} + \mu_{fg1}\bar{\rho}W_1 - W_3 \tag{47}$$

$$\frac{\partial \rho_g S}{\partial t} + u\frac{\partial \rho_g S}{\partial x} + \frac{\partial \rho_g v_g S}{\partial x} = \frac{1}{Le_{sm}}\frac{\partial^2 S}{\partial x^2} + \mu_{sm2}\bar{\rho}W_2 + \mu_{sm3}W_3 \tag{48}$$

$$\frac{\partial P}{\partial x} = -k_f v_g \tag{49}$$

$$P = \rho_g(1 + \delta\theta) \tag{50}$$

We assume that the ends of the sample are far enough from the reaction site to neglect their effects. Thus, we assume an infinite sample with the reaction site at $x = 0$. The boundary conditions then become:

$$x \to -\infty: \quad P = 1 \quad \theta = 0 \quad Y = 1 \quad F = 0 \quad S = 0 \quad \rho_g v_g = J \quad \rho_f = 1 \quad \rho_c = 0 \quad \rho_a = 0 \tag{51}$$

$$x \to +\infty: \quad \frac{\partial \theta}{\partial x} = 0 \quad \frac{\partial Y}{\partial x} = 0 \quad \frac{\partial F}{\partial x} = 0 \quad \frac{\partial S}{\partial x} = 0 \tag{52}$$

This full model was simulated numerically using finite difference approximations in MATLAB; results from these simulations are presented in the next section.

3 Results

This section is separated into two subsections. The first begins with an exploration of the different solutions that evolve with differing chemical parameter values and consistent numerical parameters. This is followed by an exploration of how changing the numerical time-stepping value has significant qualitative effects on the solutions that evolve that are indicative of severe limitations in the first section's explorations.

3.1 Changing Chemical Parameter Values

In this section, numerical parameter values remain unchanging across simulations, while chemical parameter values are changed to examine effects on how different solutions may evolve. These simulations use a region of length 10, spanning from -5 to 5, and a spatial resolution of 101 points. For each of these simulations, a sigmoidal function is used to arrange these points to have a higher density around $x = 0$, where we define the reaction to be happening. The size of each time-step, dt, is kept constant at $9e-6$. A table summarizing all chemical parameter changes is included in the Appendix (**Tables 1** and **2**). The effects of varying the time-step size are explored in **Section 3.2**.

3.1.1 Solution Types

With this constant time-stepping value, it was found that the model was able to support pyrolysis/fuel oxidation, smoldering, and flaming solutions, that can be seen in **Figures 1, 2**, and **3**, respectively.

Figure 1 shows a solution with a high rate of reaction (1) and low rates of reactions (2) and (3) at the reaction zone, characteristic of a pyrolysis and fuel oxidation solution. Char and flammable gas are created and are not meaningfully consumed.

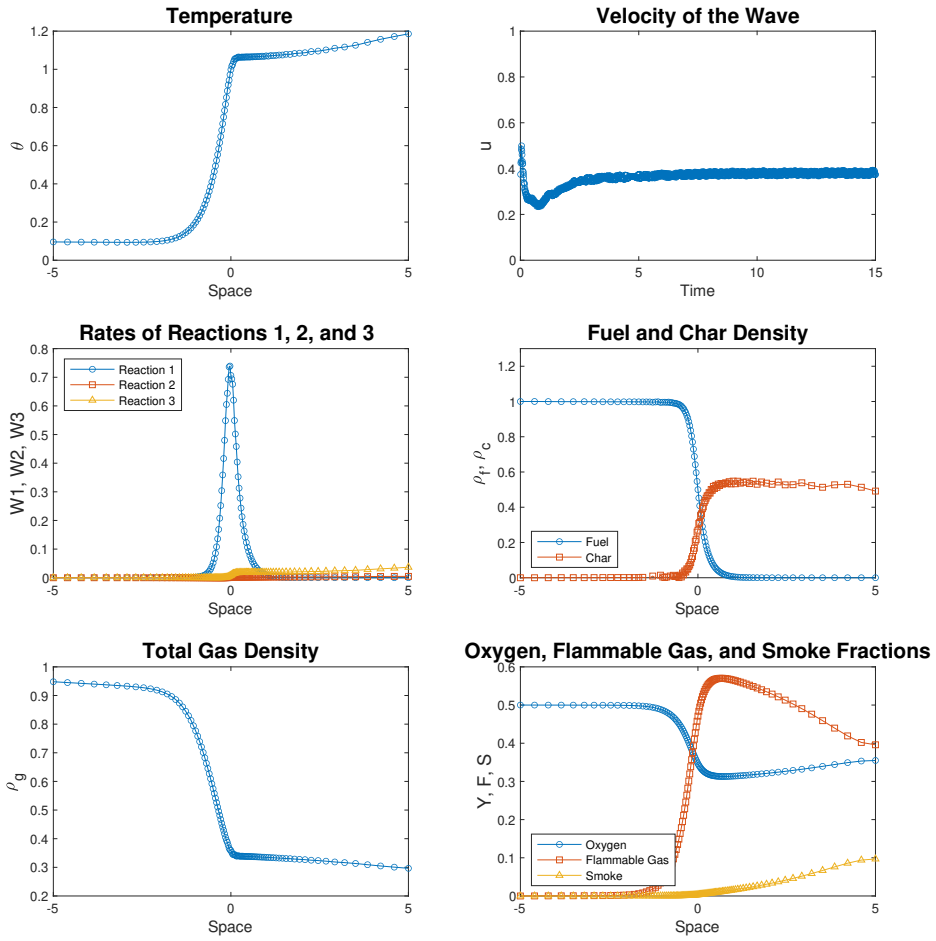

Figure 1: A pyrolysis and fuel oxidation solution. Parameter values used for this simulation are: $Z_1 = 4$, $Z_2 = 6$, $Z_3 = 10$, $Kr_{2,1} = 0.01$**, $Kr_{3,1} = 0.05$**, $c_a = c_c = 1$, $c_{ox} = c_{fg} = c_{sm} = 1$, $\bar{\rho} = \bar{c} = 2$, $Q_1 = 0.05$**, $Q_2 = 0.1$**, $Q_3 = 0.5$**, $Le_{ox} = Le_{fg} = Le_{sm} = 1.5$, $\mu_{a2} = 0.75$, $\mu_{fg1} = 1$**, $\mu_{ox1} = 0.1$, $\mu_{sm2} = 0.5$, $\mu_{sm3} = 0.5$ $k_f = 0.01$, $\delta = 2$, $Y_0 = 0.5$, and $J = 1$. All other chemical parameters can be calculated from these. Only starred parameters differ from those that lead to different solution types in **Figures 2** and **3**.

Figure 2 shows a solution with high rates of reactions (1) and (2) and a low rate of reaction (3) at the reaction zone, characteristic of a smoldering solution. The speed of the propagating wave seems to remain steady just above 0.1, and the temperature to the right of the reaction zone seems to be approximately 0.6. Char and a small amount of flammable gas are produced by reaction (1), and much of the char is consumed in reaction (2), creating a smoldering wave. A small stoichiometric coefficient ($\mu_{fg1} = 0.02$) of flammable gas produced per unit solid burned in reaction (1) limits flaming, as does the low temperature of the system.

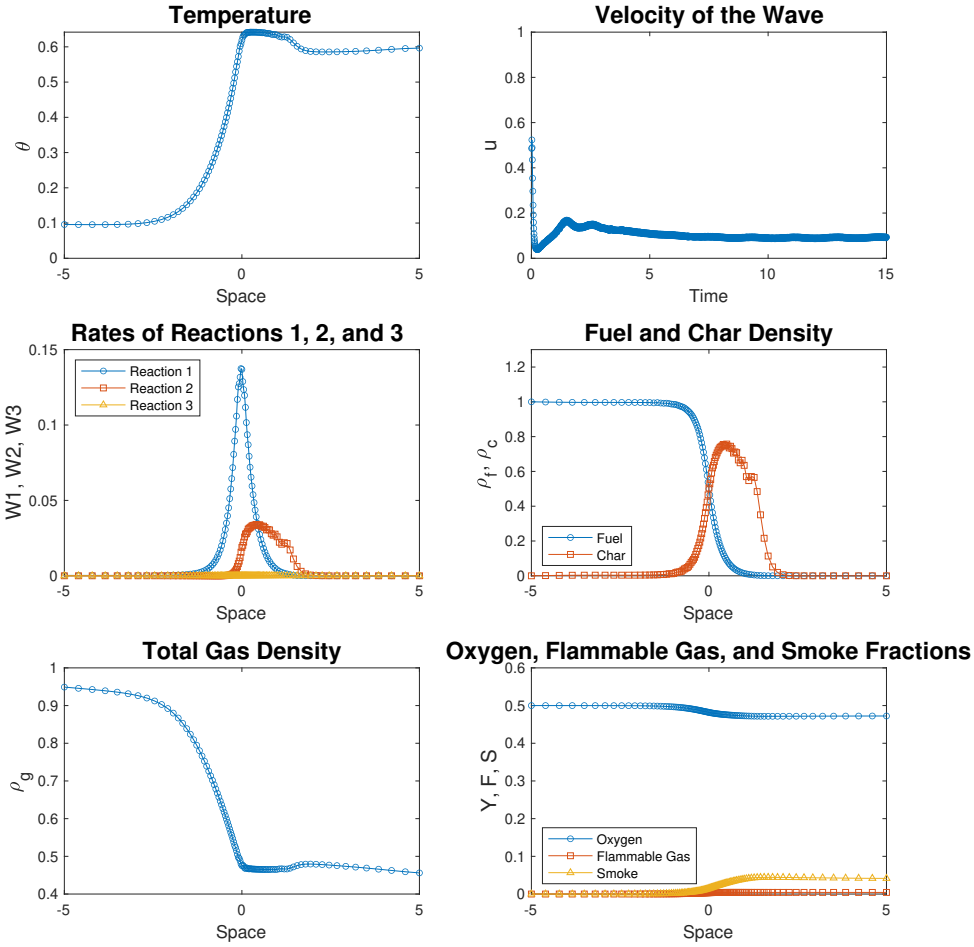

Figure 2: A smoldering solution. Parameter values used for this simulation are: $Z_1 = 4$, $Z_2 = 6$, $Z_3 = 10$, $Kr_{2,1} = 1.5$**, $Kr_{3,1} = 2.5$**, $c_a = c_c = 1$, $c_{ox} = c_{fg} = c_{sm} = 1$, $\bar{\rho} = \bar{c} = 2$, $Q_1 = 0.05$**, $Q_2 = 0.1$**, $Q_3 = 0.5$**, $Le_{ox} = Le_{fg} = Le_{sm} = 1.5$, $\mu_{a2} = 0.75$, $\mu_{fg1} = 0.02$**, $\mu_{ox1} = 0.1$, $\mu_{sm2} = 0.5$, $\mu_{sm3} = 0.5$ $k_f = 0.01$, $\delta = 2$, $Y_0 = 0.5$, and $J = 1$. All other chemical parameters can be calculated from these. Only starred parameters differ from those that lead to different solution types in **Figures 1** and **3**.

Figure 3 shows a solution with high rates of reactions (1) and (3) and a lower (but still significant) rate

of reaction (2) at the reaction zone, characteristic of a flaming solution. The speed of this wave seems to become steady at a value just above 0.4, which is notably faster than the smoldering solution (just above 0.1). Similarly, the temperature of the system for this flaming solution is higher than that of the smoldering, around 1.4.

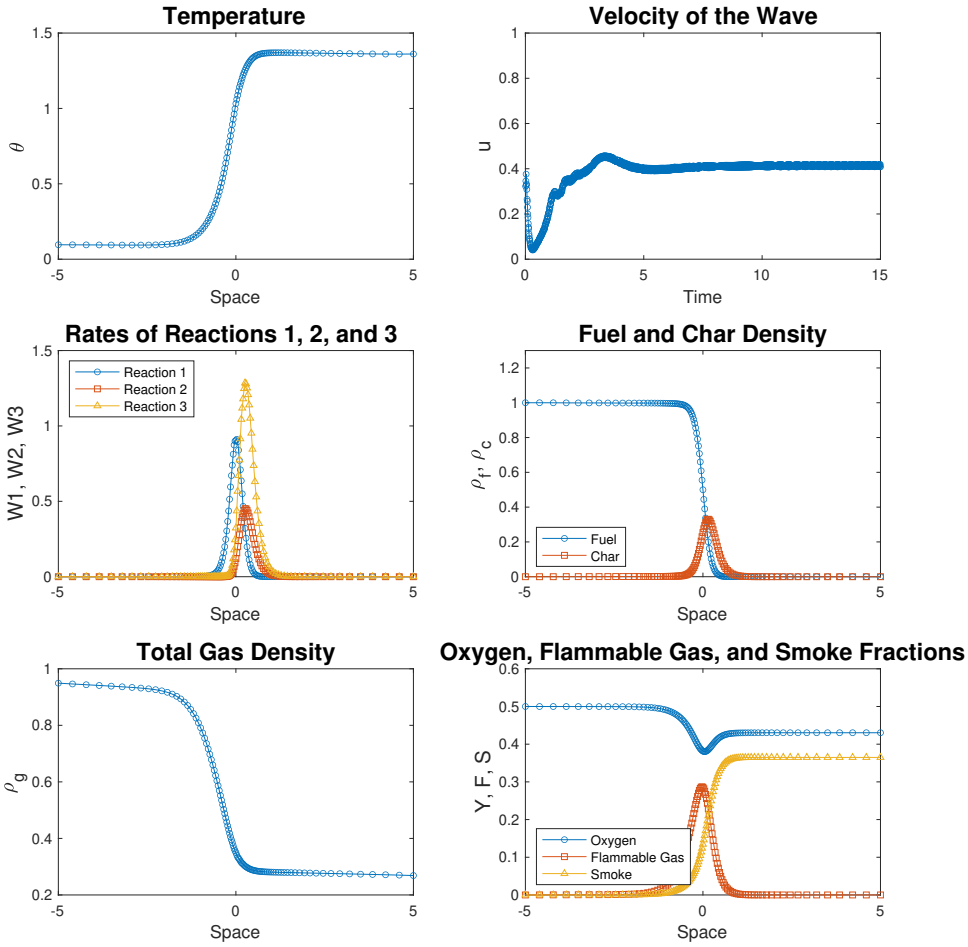

Figure 3: A flaming solution. Parameter values used for this simulation are: $Z_1 = 4$, $Z_2 = 6$, $Z_3 = 10$, $Kr_{2,1} = 1^{**}$, $Kr_{3,1} = 2^{**}$, $c_a = c_c = 1$, $c_{ox} = c_{fg} = c_{sm} = 1$, $\bar{\rho} = \bar{c} = 2$, $Q_1 = 0.1^{**}$, $Q_2 = 0.2^{**}$, $Q_3 = 1^{**}$, $Le_{ox} = Le_{fg} = Le_{sm} = 1.5$, $\mu_{a2} = 0.75$, $\mu_{fg1} = 1^{**}$, $\mu_{ox1} = 0.1$, $\mu_{sm2} = 0.5$, $\mu_{sm3} = 0.5$ $k_f = 0.01$, $\delta = 2$, $Y_0 = 0.5$, and $J = 1$. All other chemical parameters can be calculated from these. Only starred parameters differ from those that lead to different solution types in **Figures 1** and **2**.

Figure 4 shows another, more dramatic flaming solution. Each of the reactions are happening at a much higher rate in a much hotter system than in any of the previous solutions. The model fails to keep up numerically and becomes singular after 1.5776 seconds of simulated time. Further increasing the parameters

controlling the heat of each reaction (Q_1, Q_2, and Q_3) distinguishes this solution from the previous flaming solution (**Figure 3**).

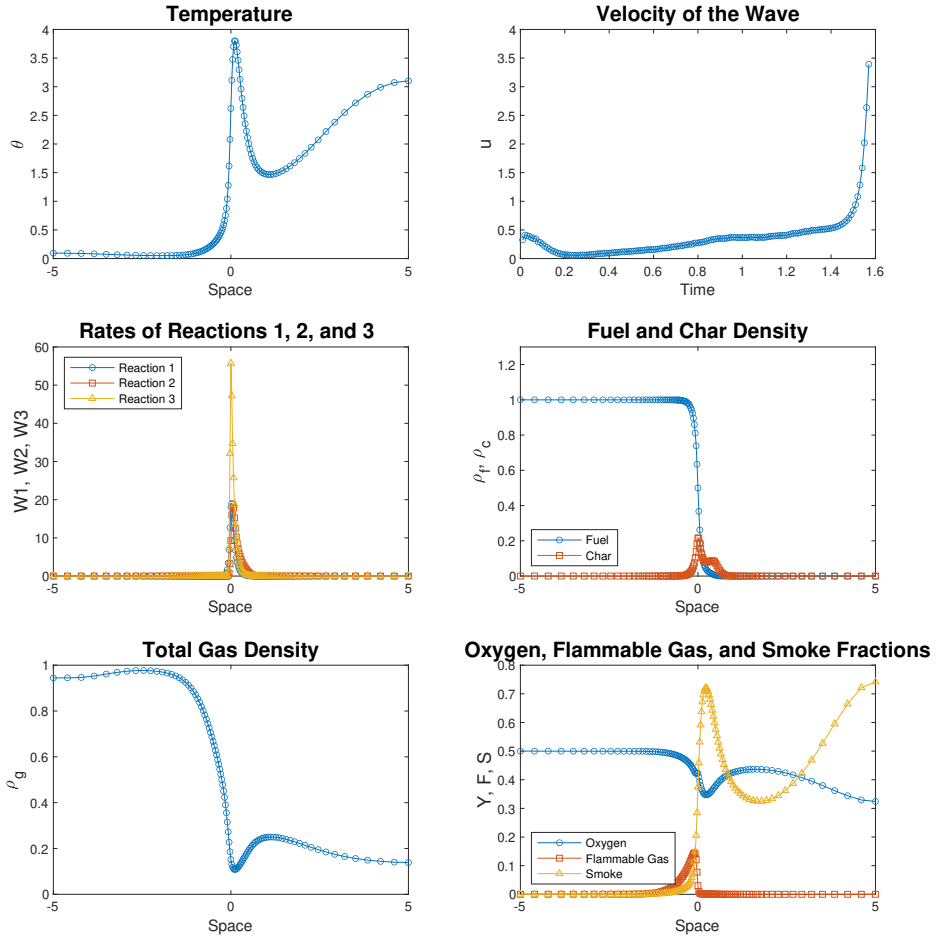

Figure 4: A more dramatic flaming solution. Parameter values used for this simulation are: $Z_1 = 4$, $Z_2 = 6$, $Z_3 = 10$, $Kr_{2,1} = 1$, $Kr_{3,1} = 2$, $c_a = c_c = 1$, $c_{ox} = c_{fg} = c_{sm} = 1$, $\bar{\rho} = \bar{c} = 2$, $Q_1 = 0.25^{**}$, $Q_2 = 0.5^{**}$, $Q_3 = 2.5^{**}$, $Le_{ox} = Le_{fg} = Le_{sm} = 1.5$, $\mu_{a2} = 0.75$, $\mu_{fg1} = 1$, $\mu_{ox1} = 0.1$, $\mu_{sm2} = 0.5$, $\mu_{sm3} = 0.5$ $k_f = 0.01$, $\delta = 2$, $Y_0 = 0.5$, and $J = 1$. All other chemical parameters can be calculated from these. Only the starred heats of reactions differ from the flaming solution shown in **Figure 3**.

Reactions (2) and (3) were encouraged (in **Figures 2** and **3**) by increasing the reaction ratios, $Kr_{2,1}$ and $Kr_{3,1}$. Decreasing μ_{fg}, the stoichiometric coefficient of flammable gases produced in pyrolysis per unit solid burned, discouraged flaming, as is expected physically. Higher heats of release, Q_1, Q_2, and Q_3, encouraged flaming in a similarly physically expected way.

3.1.2 Effects of Differing Gas Heat Capacities

Figure 5 presents the solution that evolves from the same chemical and numerical parameters used to create the pyrolysis/fuel oxidation solution presented in **Figure 1** but with differing specific heat capacities defined for oxygen, flammable gases, smoke, and inert gases. These changes seem to somewhat significantly affect the system. The system reaches a higher temperature (2.5 maximum, whereas with equal heat capacities, 1.6 maximum), and allows reaction (3) to occur more significantly. The speed of the wave is also moderately faster, seeming to become steady at a speed of 0.6 rather than 0.4, as with equal gas specific heat capacities.

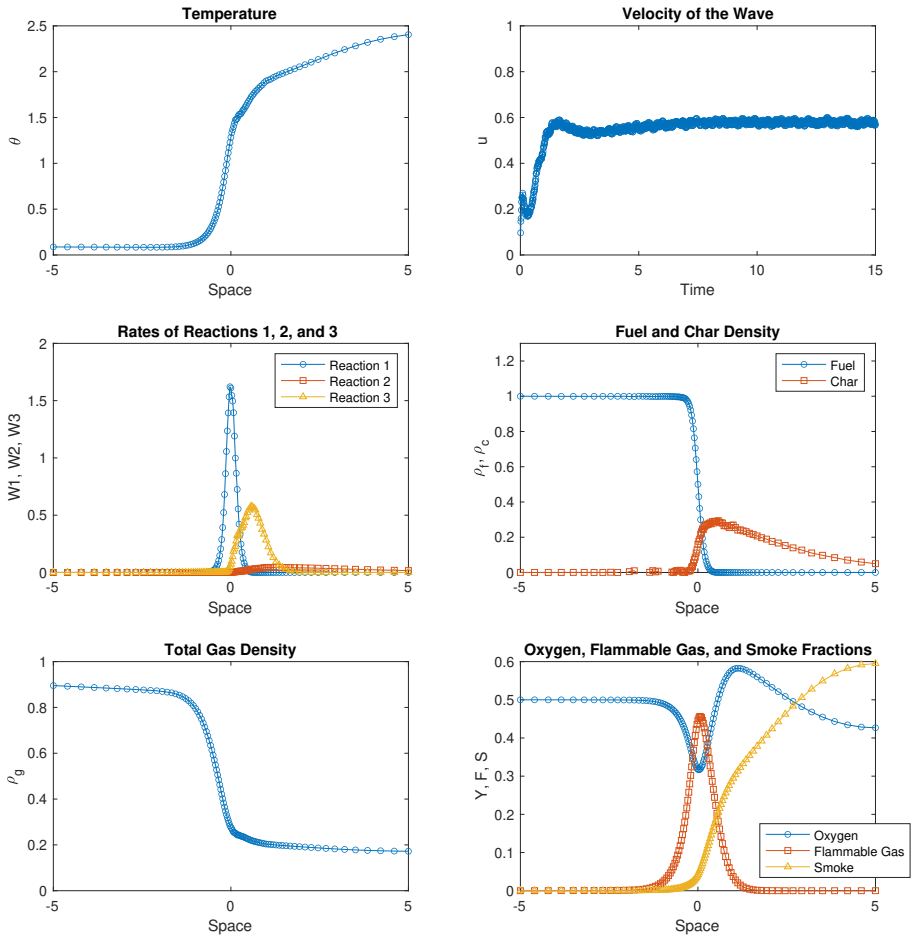

Figure 5: Pyrolysis/Fuel oxidation solution created with equal chemical and numerical parameters as those used in **Figure 1** except $c_{ox} = 0.9, c_{fg} = 1.5$, and $c_{sm} = 1.2$.

Figure 6 analogously presents the smoldering solution in **Figure 2** with these same changed gas heat capacities. In the case of smolder, these different parameters seem to have only minor quantitative effects. The solution profile looks very similar to the equal heat capacity case, with no significant changes to temperature, speed, or reaction rates.

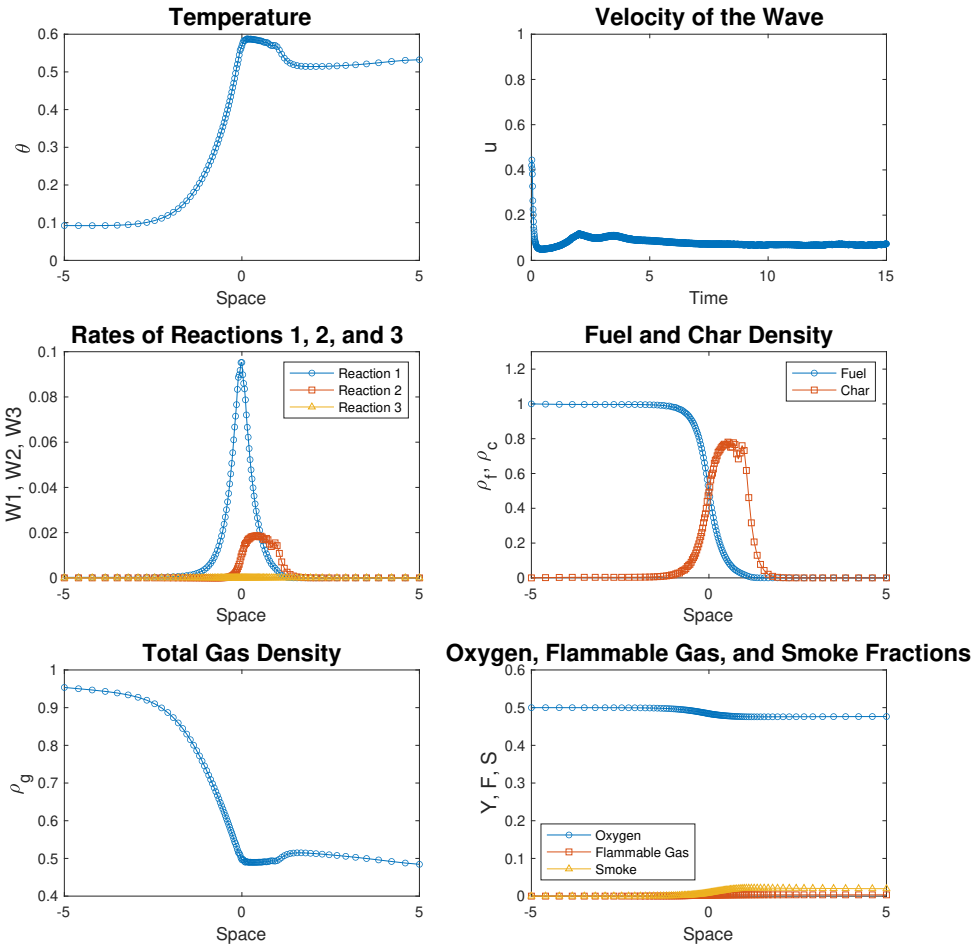

Figure 6: Smoldering solution created with equal chemical and numerical parameters as those used in **Figure 2** except $c_{ox} = 0.9, c_{fg} = 1.5$, and $c_{sm} = 1.2$.

With the flaming solution presented in **Figure 3**, it was found that this consideration of unequal gas specific heat capacities qualitatively changed the solution from a more steady type of flame to a more dramatic one, with higher temperature, wave speed, and rates of reactions, shown in **Figure 7**.

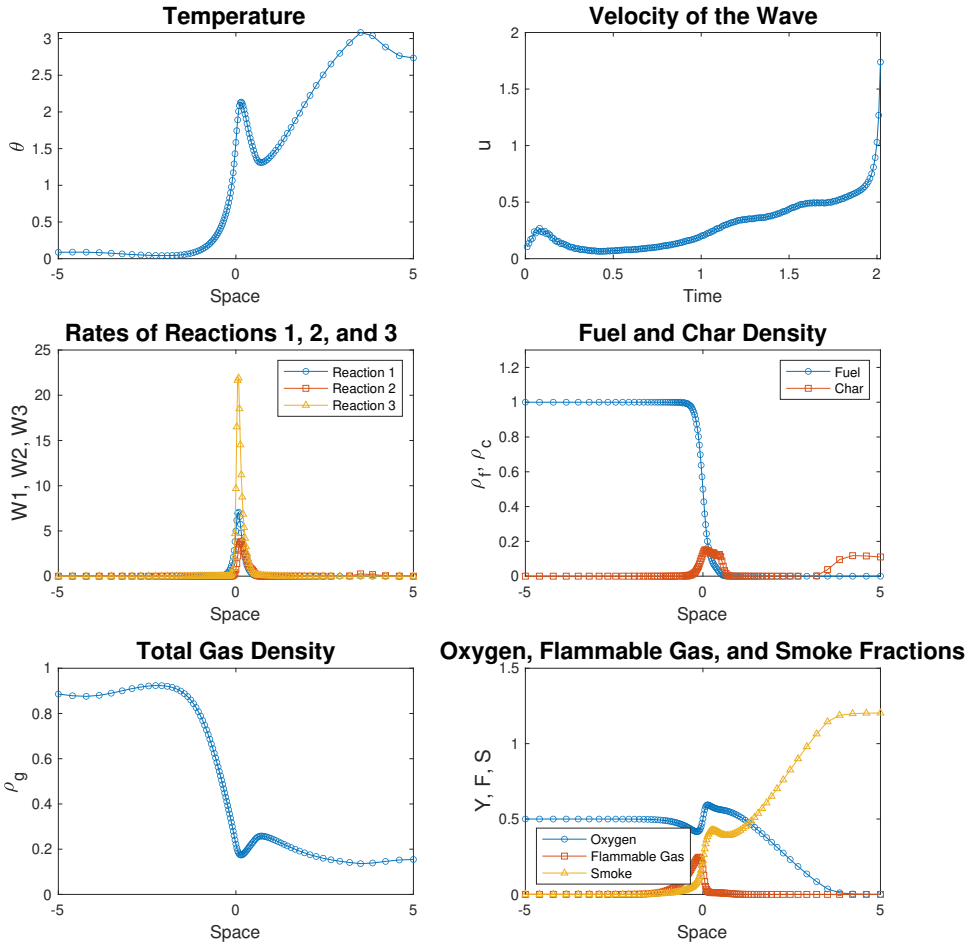

Figure 7: Dramatic flaming solution created with equal chemical and numerical parameters as those used in the more sustained flaming shown in **Figure 3** except $c_{ox} = 0.9, c_{fg} = 1.5$, and $c_{sm} = 1.2$. After 2.0383 simulated seconds, the system became singular and the model failed to simulate further.

3.2 Changing Numerical Parameter Values

Although these physically expected effects were found for the constant time-step value $dt = 9e-6$, this may be an irrelevant case, as changing this time-step size can dramatically change solutions, both quantitatively and qualitatively.

Figure 8 presents a series of pyrolysis/fuel oxidation solutions that use all identical parameters except the step size, which decreases in increments of $5e-7$ from $1e-5$ to $7e-6$. For the larger time-step sizes, reaction (1) happens on a meaningful scale, while for smaller, no reactions happen meaningfully.

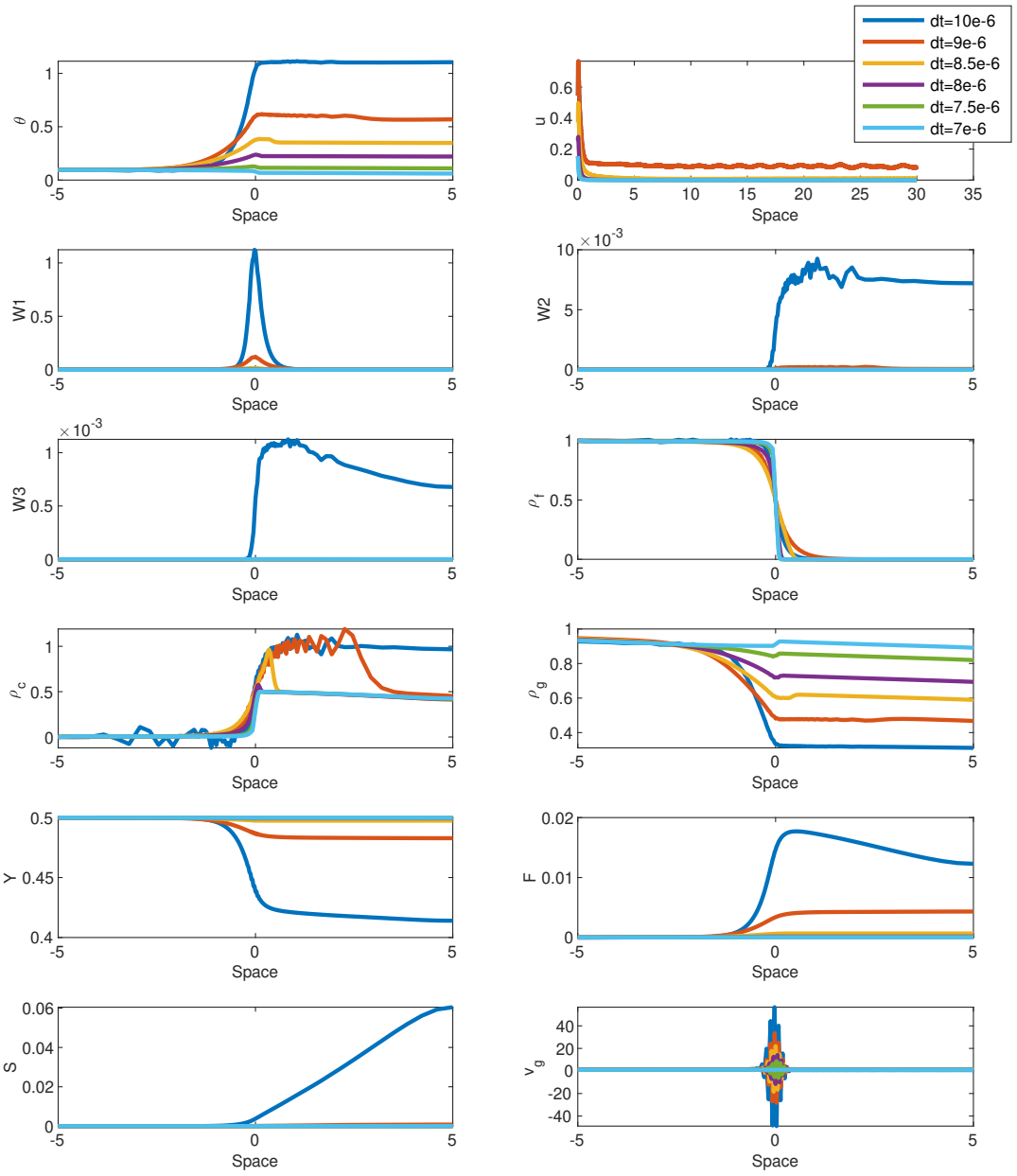

Figure 8: Pyrolysis/Fuel oxidation solutions with constant chemical parameter values and changing time-step sizes from $dt = 9e-6$ to $dt = 6e-6$ in increments of $5e-7$.

Figure 9 presents the wave speeds of solutions that evolve from the same chemical parameters as in **Section 3.1.1** but when the time-step size is decreased after 2.5 seconds (from $dt = 9e-6$ to $dt = 1e-6$). In

each of these solution types, it can be seen that the speed of the propagating wave decreases significantly with the change of step-size. Solution profiles of the temperature and reactant/product densities also qualitatively change with this decreased step size (can be seen in Appendix **Figure 10**).

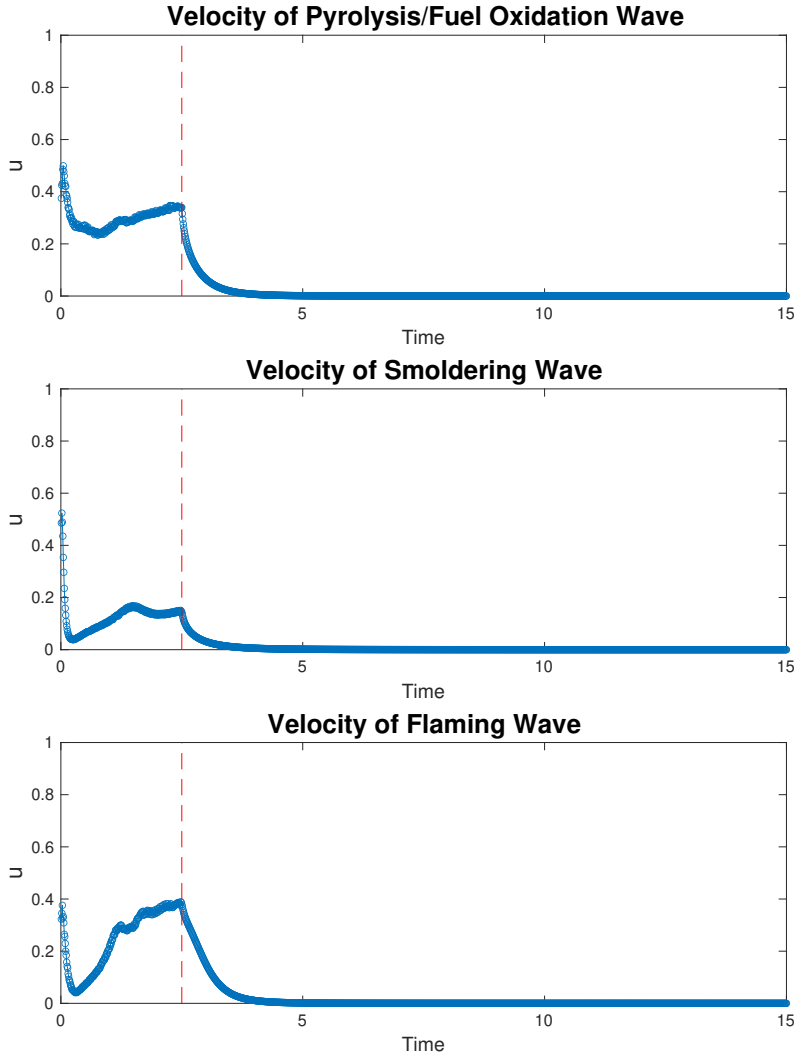

Figure 9: Pyrolysis/Fuel oxidation (top), smoldering (middle), and flaming (bottom) solutions, with time-step size changed from $dt = 9e-6$ to $dt = 1e-6$ at $t = 2.5$ (shown with dashed red line on wave speed plots). All chemical parameters for the pyrolysis/fuel oxidation, smoldering, and flaming solutions are equal to those used in **Figures 1, 2** and **3**, respectively.

4 Discussion

It was found that, in the limited case of one constant time-stepping value, pyrolysis, smoldering, and flaming solutions can evolve for different chemical parameter values that match some physical expectations in terms

of relative temperatures, speeds, and rates of reactions; found flaming combustion waves moved more quickly and maintained a higher temperature than smoldering waves.

Further, with this time-step size, the effects of considering different gas heat capacities were found to be somewhat significant on pyrolysis/fuel oxidation and flaming solutions, giving evidence that it may be worthwhile to incorporate this kind of consideration into smoldering and flaming models. In the pyrolysis/fuel oxidation case, unequal gas heat capacity terms causeed the system to reach a higher temperature and allowed reaction (3) to happen on a meaningful scale. In the flaming case, changing only these heat capacities caused the flaming solution to happen much more dramatically, with reaction (1) happening at approximately 20 times the rate of the equal heat capacity case. The temperature of the system increased with this change, approximately doubling.

Very close to the ending of this project, a sign change mistake was found in the coded finite difference schemes of the oxygen, flammable gas, and smoke fractions. Initial simulations with this error fixed did not seem to help the system's sensitivity to the time-step size, or to dramatically change the types of solutions that can evolve. The most necessary step in the continuation of this work is addressing this error and re-simulating existing code. Beginning steps in the process are presented in the Appendix.

Necessary further work also involves investigating the mechanism of the time-step's effect on solutions. The dramatic sensitivity of solution types on time-step size indicates that the results of differing chemical parameter values with $dt = 9e - 6$ may be irrelevant, even if the results follow physical intuitions. This is a severe limitation of the model and illustrates one difficulty in combining models of smoldering and flaming.

Something that could help with this exploration of time-stepping could be an adaptive time-stepping scheme. This could also be helpful to reduce the run-time of the simulations and to give greater resolution when needed (which could help the model to perhaps support more dramatic flaming solutions, like that presented in **Figure 4**).

Further work could also include searching for a region where smoldering and flaming solutions are bi-stable. In such a region, the same set of chemical parameters could lead to either smoldering or flaming solutions, and the type of solution that evolves would depend only on changes in the initial conditions of the system. Such a region could ultimately give further insight into the transition between smoldering and flaming.

Acknowledgements

I would like to sincerely thank Professor Schult for his generous support and guidance throughout this project.

References

[1] A. P. Aldushin, A. Bayliss, and B. J. Matkowsky. On the transition from smoldering to flaming. *Combustion and Flame*, 145:579–606, 2006.

[2] A. Bar-Ilan, O. Putzeys, and G. Rein. Transition from forward smoldering to flaming in small polyurethane foam samples. *Proceedings of the Combustion Institute*, 30(2), 2005.

[3] M. A. Decker and D. A. Schult. Dynamics of smoulder waves near extinction. *Combustion Theory and Modeling*, 8:491–512, 2004.

[4] M. L. Kelley and D. A. Schult. Modeling extinction in forced opposed flow smolder. *Combustion Theory and Modeling*, 8:491–512, 2004.

[5] Z. Lu. A diffusion-flame analog of forwarf smolder waves - (i) 1-d steady structures. *Combustion and Flame*, 196:515–528, 2018.

[6] G. Rein. Smouldering combustion phenomena in science and technology. *International Review of Chemical Engineering*, 1:3–18, 2009.

[7] M. A. Santoso, J. Yang, H. Chen, and G. Rein. Literature review on the transition from smouldering to flaming fires and its application to peat fires. *Advances in Forest Fire Research 2018*, pages 529–533, 2018.

[8] C. Schwartz. Exploring the impacts of more complex reactions on smouldering combustion. *(Unpublished)*, 2019.

[9] S. I. Stoliarov, O. Zeller, A. B. Morgan, and S. Levchik. An experimental setup for observation of smoldering-to-flaming transition on flexible foam/fabric assemblies. *Fire and Materials*, 42(1):128–133, 2018.

Appendix

Parameter Summary

Tables 1 and **2** list chemical parameter changes between the simulations shown in this paper. Each simulation used $Z_1 = 4$, $Z_2 = 6$, $Z_3 = 10$, $c_a = c_c = 1$, $\bar{\rho} = \bar{c} = 2$, $Le_{ox} = Le_{fg} = Le_{sm} = 1.5$, $\mu_{a2} = 0.75$, $\mu_{ox1} = 0.1$, $\mu_{sm2} = 0.5$, $\mu_{sm3} = 0.5$ $k_f = 0.01$, $\delta = 2$, $Y_0 = 0.5$, and $J = 1$. All other chemical parameters can be calculated from these.

	$Kr_{2,1}$	$Kr_{3,1}$	Q_1	Q_2	Q_3	μ_{fg1}
Figures 1 and 5: Pyrolysis/Fuel Oxidation	0.01	0.05	0.05	0.1	0.5	1
Figures 2 and 6: Smoldering	1.5	2.5	0.05	0.1	0.5	0.02
Figures 3 and 7: Flaming	1	2	0.1	0.2	1	1
Figure 4: Flaming (Dramatic)	1	2	0.25	0.5	2.5	1
Figure 8: Pyrolysis/Fuel Oxidation (With Changing dt)	0.01	0.05	0.05	0.1	0.5	0.02

Table 1: A summary of the different parameters that were changed to create the different solutions in Section 3.

	c_{ox}	c_{fg}	c_{sm}
Section 3.1.1, Figures 1-4 and Section 3.2, Figure 8	1	1	1
Section 3.1.2, Figures 5-7	0.9	1.5	1.2

Table 2: A summary of the different gas specific heat capacity values used

Fuller Picture of Changed Time-Step Size Effects on Solution Types

Figure 10 shows more aspects of the pyrolysis/fuel oxidation, smoldering, and flaming solution profiles found when the time-step size is changed from $dt = 9e-6$ to $dt = 1e-6$. The changes with a smaller-step size are not just in scale; the wave speeds are much slower, with lower temperature and reaction rates, and also the profiles of temperature and total gas mass are different in shape (a "mirrored" sort of shape from in the $dt = 9e-6$ case).

Pyrolysis and Fuel Oxidation

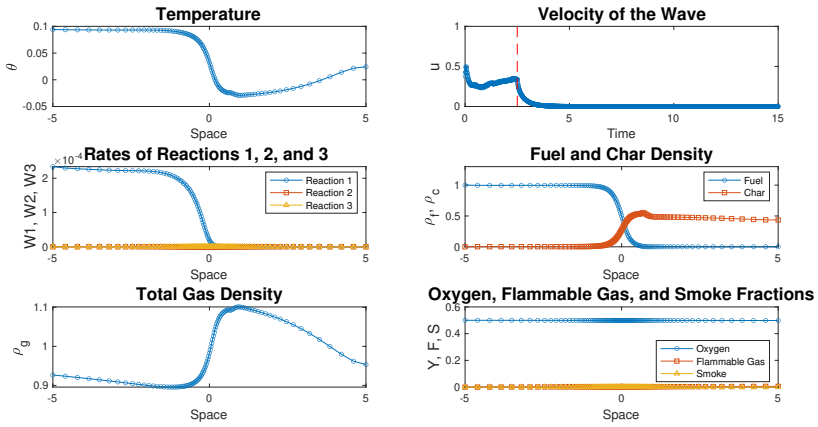

Smoldering

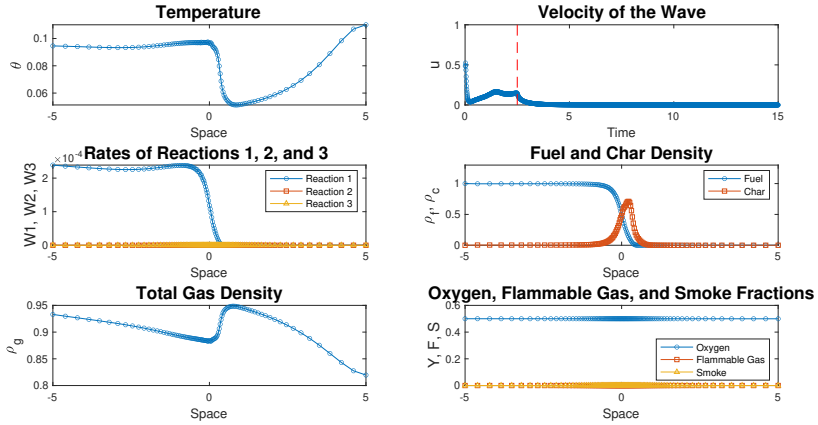

Flaming

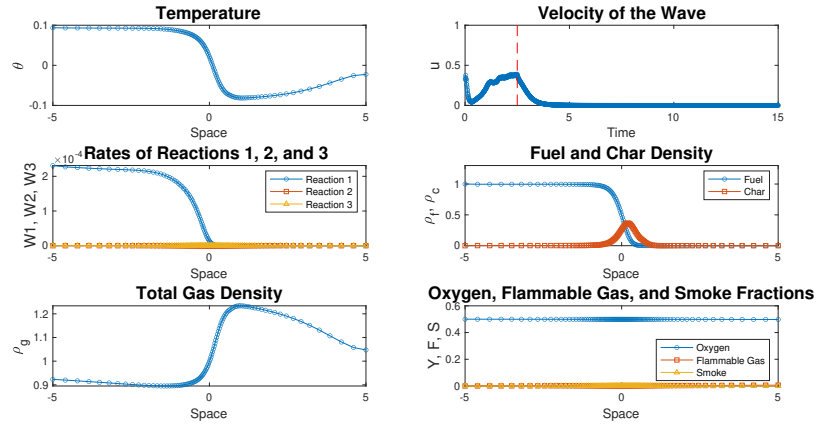

Figure 10: Pyrolysis/Fuel oxidation (top), smoldering (middle), and flaming (bottom) solutions, with time-step size changed from $dt = 9e-6$ to $dt = 1e-6$ at $t = 2.5$ (shown with dashed red line on wave speed plots). All chemical parameters for the pyrolysis/fuel oxidation, smoldering, and flaming solutions are equal to those used in **Figures 1, 2** and **3**, respectively.

Addressing Code Error

Figures 11-13 present some of the same simulations conducted in the paper with the sign change error addressed. It seems the the parameters that lead to smoldering as discussed in the paper lead to smoldering again, but this is not true of the pyrolysis/fuel oxidation and flaming solutions. An initial guess is because the parameter μ_{fg_1} is very small for the smoldering solution, and significantly bigger for the other two.

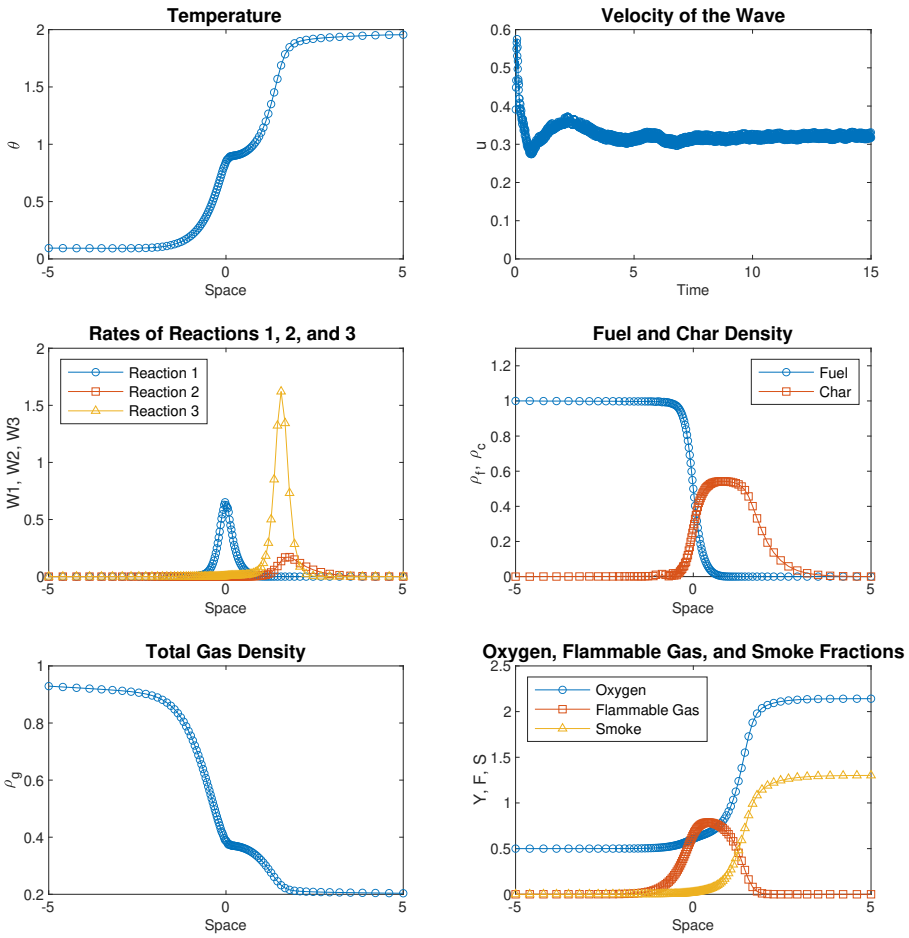

Figure 11: Figure 1 run with corrected code.

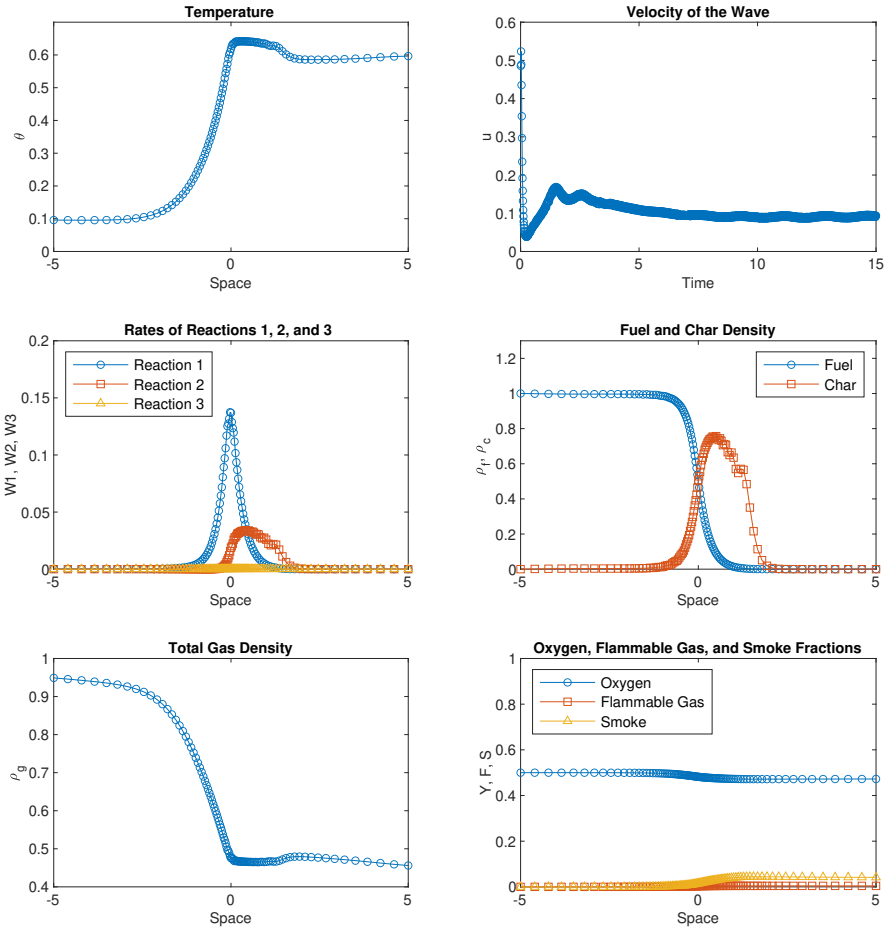

Figure 12: Figure 2 run with corrected code.

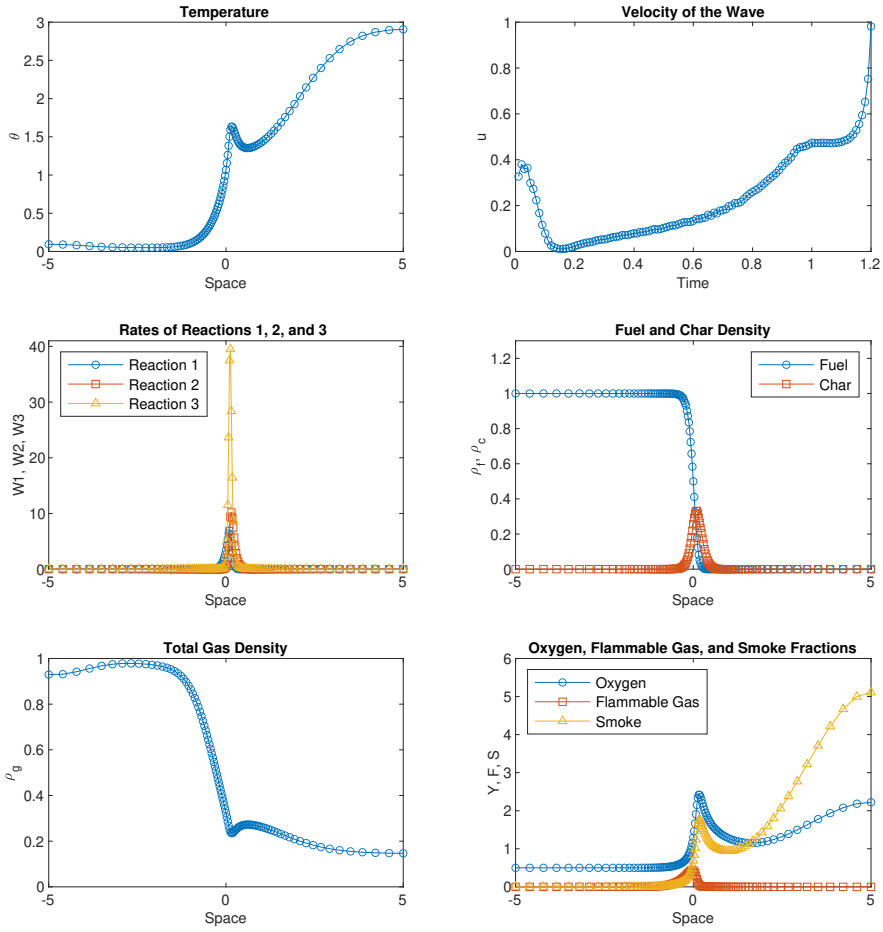

Figure 13: Figure 3 run with corrected code.

For the smoldering solution, results follow as they did in the paper with no obvious differences. **Figure 14** presents the analogous unequal heat capacity exploration, and **Figure 15** presents the analogous time-step size exploration with the fixed code.

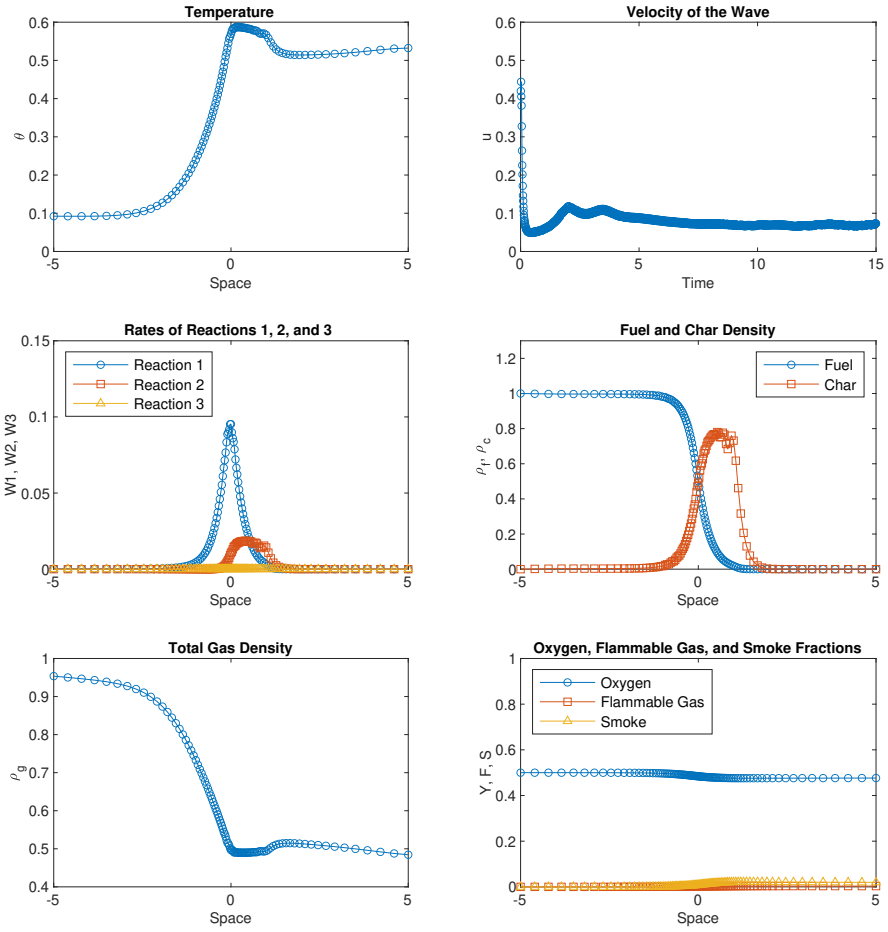

Figure 14: Figure 6 run with corrected code.

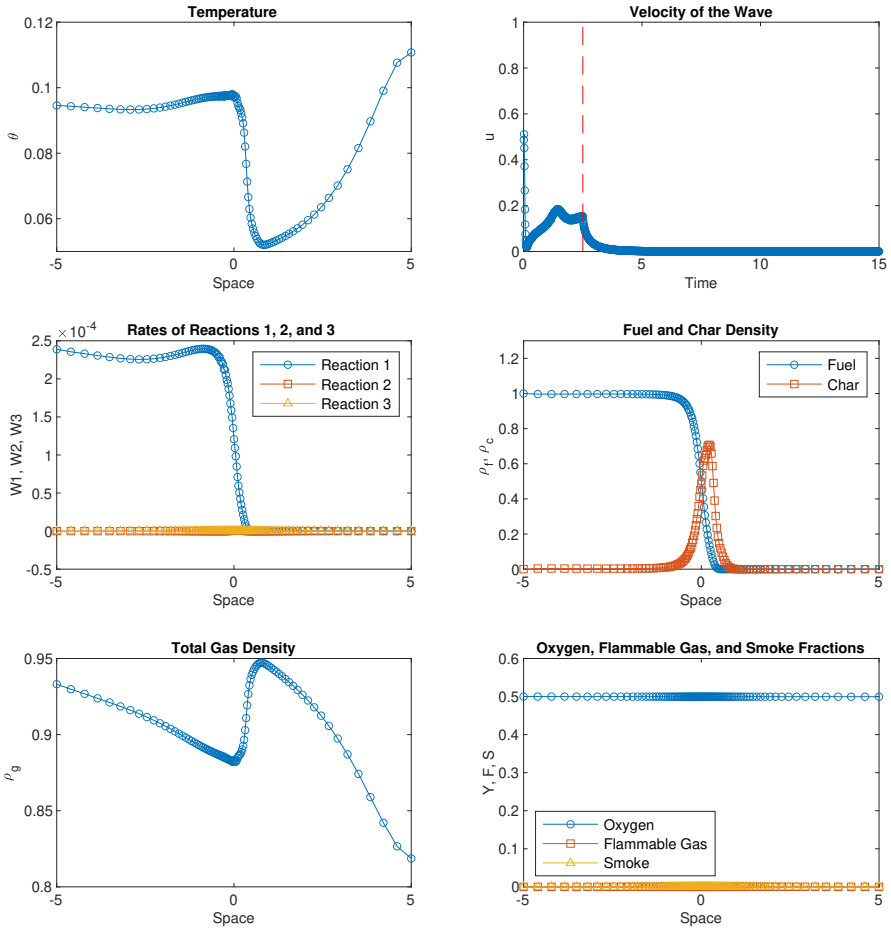

Figure 15: The smoldering solution in **Figure 10** run with corrected code.

The next step in continuing this work is exploring this new parameter space more thoroughly to see if pyrolysis/fuel oxidation and flaming solutions are similarly supported, and if the results discussed in the paper hold.